Available online at www.sciencedirect.com
SCIENCE DIRECT®
Optics Communications 258 (2006) 114–134
OPTICS COMMUNICATIONS
www.elsevier.com/locate/optcom

Theoretical analysis and performance investigation of ultrafast all-optical Boolean XOR gate with semiconductor optical amplifier-assisted Sagnac interferometer

K.E. Zoiros [a,*], G. Papadopoulos [a], T. Houbavlis [a], G.T. Kanellos [b]

[a] *Lightwave Communications Research Group, Department of Electrical and Computer Engineering, Democritus University of Thrace, 12 Vas. Sofias Str., 67 100, Xanthi, Greece*
[b] *Photonics Communications Research Laboratory, Department of Electrical and Computer Engineering, National Technical University of Athens, 9 Iroon Polytechniou Str., 157 73, Athens, Greece*

Received 31 May 2005; accepted 25 July 2005

Abstract

A comprehensive theoretical model of an ultrafast all-optical Boolean XOR gate implemented with a semiconductor optical amplifier (SOA)-assisted Sagnac interferometer is presented. The model accounts for the SOA small signal gain, linewidth enhancement factor and carrier lifetime, the switching pulses energy and width and the Sagnac loop asymmetry. By undertaking a detailed numerical simulation, the influence of these key parameters on the metrics that determine the quality of switching is thoroughly investigated and simple design rules are extracted for their proper selection so as to ensure optimum operation. The obtained results are in good agreement with the published experimental measurements and confirm the feasibility of realizing the gate at 10 Gb/s with fairly high performance. The model can be extended for studying more complex all-optical circuits of enhanced functionality in which the XOR gate is the basic building block.

Keywords: All-optical Boolean XOR logic; All-optical signal processing; All-optical switching; Semiconductor optical amplifier (SOA); SOA-assisted Sagnac interferometer

1. Introduction

In recent years, the remarkable progress in photonics technology [1] and the efficient combination of wavelength division multiplexing (WDM) and optical time division multiplexing (OTDM)

* Corresponding author. Tel.: +30 25410 79 975; fax: +30 25410 79 595.
E-mail address: kzoiros@ee.duth.gr (K.E. Zoiros).

0030-4018/$ - see front matter © 2005 Elsevier B.V. All rights reserved.
doi:10.1016/j.optcom.2005.07.059

techniques [2] has made feasible the development of high capacity optical telecommunications networks. Although this achievement has essentially resolved the issue of transmission in the optical layer, at the same time it is not sufficient from a practical point of view given that in the rapidly changing broadband environment of Internet and multimedia applications a network must be capable of offering high quality, flexible and scaleable bandwidth-on-demand services to satisfy the various users' needs. This fact renders imperative the adoption of the all-optical signal processing technological approach [3], which can handle information exclusively in the optical domain so that cumbersome, complex and power-consuming optical–electrical–optical (O/E/O) conversions are avoided and the cost per connected bit transmitted is kept low. In this context, the all-optical Boolean XOR gate has been identified as the key element for realizing a set of important networking functions such as bit pattern recognition [4], address comparison [5], label swapping [6], pseudorandom binary sequence generation and encryption [7], binary addition [8] and bit parity checking [9]. For this reason, all-optical XOR logic has attracted considerable research interest during the recent years and many results have been reported in this field exploiting either the nonlinearity of optical fibers [4,10,11] or of a semiconductor optical amplifier (SOA) [12–21]. Fiber-based XOR gates utilize the Kerr effect and have the potential of operating at ultra-high speed due to the very short relaxation times (<100 fs) of the nonlinearity, which is essentially instantaneous. Nevertheless, this nonlinearity is weak so that long interaction lengths and high switching energies are required for adequate performance, which results in unacceptable processing time delays, in a large physical size of the gate that impedes its practical use and in poor power efficiency. SOAs, on the other hand, are characterized by a nonlinearity that is four orders of magnitude higher than fiber's, which relaxes the energy requirements, reduces the time-of-the flight of the gate and enables stable, efficient and cascadable operation in a real ultra-high speed optical communications environment [22]. The most important advantage of SOAs, however, is their integration potential, which results in compact, reliable and cost effective implementations and consequently opens the road for mass production and commercial availability [23]. The nonlinear effects in SOAs have been appropriately exploited for the demonstration of all-optical XOR logic using self-phase modulation (SPM) [12], cross-gain modulation [13], cross-polarization modulation [14], four-wave mixing [15], simultaneously four-wave mixing and cross-gain modulation [16] and cross-phase modulation in various interferometric configurations such as the ultrafast nonlinear interferometer [17] and the Mach–Zehnder interferometer (MZI) [18–21], which has been also theoretically studied [24–28]. Except from these two SOA-based configurations, another type of interferometer is the SOA-assisted Sagnac switch/terahertz optical asymmetric demultiplexer (TOAD) that effectively combines the fast switching time, low switching energy, low latency and reasonable noise figure with the integration potential and overall practicality, which enable it to compete favourably with other similar OTDM devices [29]. Despite these attractive features and the fact that the all-optical XOR operation has been experimentally demonstrated with this switch at 10 [30] and 20 Gb/s [31], its performance has not been extensively analyzed and investigated. Instead, the theoretical studies have been restricted to the AND gate or equivalently to the demultiplexing function [32–34] and only recently a novel scheme of all-optical XOR logic based on a Sagnac interferometer was numerically simulated, using however two SOAs in order to overcome the speed limitation imposed by the gain recovery time and eliminate the associated pattern effect, which inevitably increase the device's complexity [35]. In this paper, we explore the ability of the SOA-assisted Sagnac switch to perform Boolean bitwise XOR logic between optical signals that carry 10 Gb/s data information. For this purpose, a complete and robust model is developed and appropriately applied to the case of the specific XOR gate. It consists of a set of equations that describe propagation and amplification of optical pulses through a SOA in an interferometric switch as well as the interaction of the SOA carriers with an intense optical field. The numerical solution of these equations allows to study and

evaluate the influence of the critically involved parameters, which include the SOA small signal gain, linewidth enhancement factor and carrier lifetime, the switching pulses energy and width and the Sagnac loop asymmetry, on the defined performance metrics and to appropriately select them so as to ensure optimum operation. The obtained results can provide a helpful tool for the design and implementation of all-optical semiconductor-based XOR gates and their exploitation in more complex all-optical signal processing circuits in which they are the core logic unit.

2. Principle of operation

The operation of the SOA-assisted Sagnac XOR gate can be described with the help of the simplified diagram of Fig. 1, which consists of an optical loop mirror and a SOA placed asymmetrically with respect to the center. In order to perform the Boolean XOR operation, two optical control beams A and B that may take a logical '0' and '1' enter the loop via a discriminating coupler, which can be either wavelength or polarization selective, with the latter having the advantage that the gate can be directly used in feedback applications without the need for complex wavelength conversion. A clock stream held continuously to a logical '1' enters the loop through the 3 dB coupler and is split into two equal, counter-propagating parts, the clockwise (CW) and the counter-clockwise (CCW), which due to the asymmetry reach the SOA at different times. The control pulses must arrive at the SOA just before their corresponding co-propagating clock components and their energy must be at least ten times higher than that of the clock pulses so that only them can modify the SOA dynamic optical properties, which are subsequently suffered by the clock [36]. Provided that these timing and energy conditions are satisfied, the XOR function can be properly executed as it can be explained with the help of the simple example shown in Fig. 2, in which a representative binary frame $A = \{A_1, A_2, A_3, A_4\} = \{1,1,0,0\}$ and $B = \{B_1, B_2, B_3, B_4\} = \{1,0,1,0\}$ has been isolated in time for illustration purposes. More specifically, when both A and B are '1', then pulse $\{A_1\} = \{1\}$ that is inserted first in the SOA depletes its carrier density, thereby changing significantly its refractive index and saturating strongly its gain. This in turn causes a phase shift through cross-phase modulation on the CW1 clock component that arrives at the SOA just after the control. The counter-propagating control pulse, $\{B_1\} = \{1\}$, has a similar effect on the SOA gain properties and induces almost the same phase shift on the CCW1 clock component so that no phase difference is created between the clock parts. When these recombine thus at the input coupler, no signal appears at the output port of the gate, which verifies that '1' XOR '1' = 0. With the advent of the next pair of bits, $\{A_2, B_2\} = \{1,0\}$, the CW2 pulse experiences again a saturated gain, whilst its CCW2 counterpart that arrives in the SOA after a relative delay due to the asymmetry a partially recovered gain. In this way, a substantial gain difference and hence a differential phase shift is created between the two clock components so that they interfere constructively when they return at the coupler and a signal is produced at the output. The opposite occurs for the third pair of bits, $\{A_3, B_3\} = \{0,1\}$, which is the conjugate of the preceding one, so that the CW3 pulse sees a gain that has had the time to significantly recover due to the

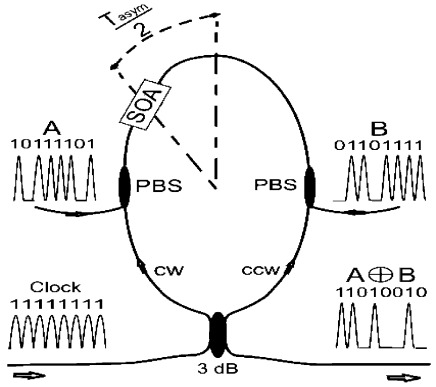

Fig. 1. Configuration of all-optical XOR gate with SOA-assisted Sagnac interferometer. A and B: Control streams carrying 10 Gb/s modulated data between which the XOR operation ($A \oplus B$) is performed, CW and CCW: clockwise and counter-clockwise components, respectively, obtained after the inserted clock stream (Clock) is split by a 3 dB coupler, T_{asym}: time asymmetry between the CW and CCW parts determined by the SOA offset from the midpoint of the loop, PBS: polarization beam splitter for discriminating the clock and control pulses using orthogonal polarization.

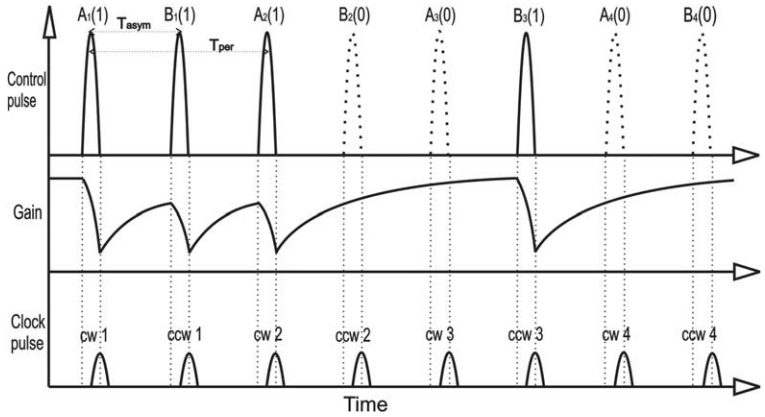

Fig. 2. Simplified diagram showing the evolution in time of the XOR operation between the four logical combinations of data patterns A and B and the corresponding SOA gain suffered by the CW and CCW clock parts. Note that the order of the pairs of bits has been arbitrarily chosen and that the synchronization of the XOR gate can be experimentally adjusted using an intraloop optical delay line so that the CW and CCW clock components arrive just after controls A and B [30,31], respectively.

succession of the zero bit, $\{B_2\} = \{0\}$, in the previous bit pair and of the zero, current bit, $\{A_3\} = \{0\}$, whilst the CCW3 pulse sees a gain that is strongly saturated by $\{B_3\} = \{1\}$. This essentially means that when either control is '1', it is mapped on the clock signal that exits the gate so that '1' XOR '0' = 1 and vice versa is achieved. Finally, in case that both controls are absent, or equivalently their data content is '0', then both CW4 and CCW4 parts will experience almost the same level of recovered gain so that the Sagnac interferometer is balanced and its switching state remains unchanged resulting in a zero output. This procedure is similarly repeated between the continuously arriving bits of the two data patterns producing a '0' if they are identical and a '1' if they differ so that the XOR truth table of Table 1 can be correctly realized for the four logical combinations of A and B.

The time difference in the arrival of the complementary clock pulses at the SOA is defined as the asymmetry, T_{asym}, which is twice the temporal offset of the SOA from the fiber loop centre (i.e. $T_{\text{asym}} = 2 \times \frac{T_{\text{asym}}}{2}$ according to Fig. 1) and can be practically adjusted by using an intraloop optical delay line. This parameter approximately determines the width of the gate's switching window [36] and is thus a key factor in order to achieve optimum operation. More specifically, it must be less than half the period of the clock, T_{per}, otherwise the two counter-propagating halves of the clock pulse being processed will not experience the gain dynamics caused by their synchronized control pulses but instead by others resulting in incomplete switching and wrong XOR results. An additional requirement for a clock pulse to be fully transmitted is that its width (at half maximum), T_{FWHM}, must be as short as possible and ideally less than the switching window so that when the CCW pulse is inserted in the SOA, the CW pulse has already passed through. In any other case, the two clock components will overlap inside the SOA so that its nonlinear properties will be only partially altered and the required differential phase shift will not be created. In other words, the width of the switching window cannot be shorter than the control pulse width [34,36]. Moreover, the asymmetry must be less than the SOA gain recovery time that is expressed by the carrier lifetime parameter, T_{car}. This can be better understood by considering for example the case of '0' XOR '1' in Fig. 2. As it can be seen, due to bit '0', the CW3 clock part experiences a partially

Table 1
XOR truth table

A	B	A XOR B
1	1	0
1	0	1
0	1	1
0	0	0

recovered gain so that after the gain has been saturated by bit '1', which arrives after a time equal to the asymmetry, the CCW3 pulse must enter the SOA before carrier recombination is completed in order for the necessary phase shift to be induced. The simultaneous satisfaction of all these conditions is expressed by

$$T_{\mathrm{FWHM}} < T_{\mathrm{asym}} < T_{\mathrm{per}}/2 \quad \text{and} \quad T_{\mathrm{asym}} < T_{\mathrm{car}}. \quad (1)$$

3. Model formulation and solution

The numerical study undertaken within the frame of this work aims at describing the operation of the SOA-assisted Sagnac XOR gate by reproducing the experimental conditions as realistically as possible. However, this goal cannot be achieved with a rigorous simulation model unless it is too complicated, so that certain simplifications and assumptions must be inevitably made. The first assumption is that the energy of the clock signal is so small that it does not affect the SOA gain dynamics and its counter-propagating components only probe the change of the refractive index caused by the intense control pulses. This assumption is correct since the energy of the clock signal is in practice at least 10% smaller than that of the control [36], which implies that the carrier depletion in the SOA active region due to the former is negligible and is determined only by the latter. In this manner, the mathematical expressions of the gain and phase responses can be greatly simplified, which otherwise would require to take into account the optical nonlinearities induced by the interaction of the control and clock pulses as well as by the overlapping between the clock counterparts. Furthermore, the effect of amplified spontaneous emission (ASE) is neglected for three main reasons, namely because (a) the SOA is essentially operated in deep saturation due to the simultaneous presence of the two control beams so that the influence of ASE is relatively small and results in insignificant changes in the gate's performance, (b) the level of ASE becomes high enough and influences the gain saturation only for SOAs longer than 1500 μm and for low repetition rates that leave ASE more time to recover between successive control pulses [37], which however is not the case in this paper, and (c) by designing the SOA so as to provide sufficient gain and by operating it near the optimal saturation point, the signal-to-noise ratio (SNR) of the Sagnac switch can be significantly enhanced [38]. Moreover, for pulse widths below 10 ps the influence of ultrafast intraband carrier processes on nonlinear gain compression has been found to be important and must be taken into account in the description of the SOA saturation under pulsed operation [39]. However, since our interest is focused on the XOR gate operation for control pulse widths that are over the low picosecond regime and whose energy is less than 1 pJ, only the contribution of carrier heating (CH) and spectral hole burning (SHB) is dominant and hence considered, whilst the effect of two-photon absorption (TPA) and ultrafast nonlinear refraction (UNR) is neglected because it becomes significant for pulses that are hundreds of femtoseconds wide and have an energy larger than 1 pJ [40]. Furthermore, the SOA small signal gain, internal loss and saturation energy are assumed to be wavelength independent and hence the same for both control and clock pulses, otherwise the investigation of the impact of this parameter on the performance of the gate would require the use of a second-order polynomial approximation of the gain spectrum [41] that would only increase the model's complexity without offering a significant benefit regarding the qualitative interpretation of the obtained results. This fact justifies also to assume that the central frequency of the control pulses is located at the peak of the SOA gain spectrum at 1550 nm and that the frequency detuning between the control and clock signals is higher than 1 THz, so that the formed temporal gratings do not play an important role in determining the response of the SOA and their effect can be disregarded [42]. An additional approximation is that the gain and group-velocity dispersion is neglected, which is practically satisfied for pulse widths in the picosecond range and SOAs several hundreds of micrometers long [43]. This essentially means that the clock and control signals travel through the SOA at the same speed so that their transit time is equal, which in turn forms the basis for deriving the initial conditions required in the numerical

approach. Finally, it is assumed that both controls have the same polarization, which is maintained as they traverse the loop, that they have been synchronized with respect to their co-propagating clock components, that the initial phase of the CW and CCW clock pulses in the two arms of the interferometer is zero, and that the SOA is polarization independent and of traveling wave type with null facet reflectivities.

In order to analyze and investigate the performance of the SOA-assisted Sagnac XOR gate, the comprehensive model of [44] that successfully describes the operation of TOAD is appropriately applied. This model links effectively the carrier density rate equation with the equation of the electric field evolution inside a SOA that is subject to a strong optical control signal to derive the following set of partial differential equations for the gain, G, and power, P, of the control and clock signals:

$$\pm\frac{\partial P_{\mathrm{A,B}}(z,t)}{\partial z}=\left[\frac{G_{\mathrm{A,B}}(z,t)}{1+\varepsilon P_{\mathrm{A,B}}(z,t)}-\alpha_{\mathrm{int}}\right]P_{\mathrm{A,B}}(z,t), \tag{2}$$

$$\frac{\partial G_{A,B}(z,t)}{\partial t}=\frac{G_{\mathrm{ss}}-G_{\mathrm{A,B}}(z,t)}{T_{\mathrm{car}}}-\frac{G_{\mathrm{A,B}}(z,t)}{E_{\mathrm{sat}}}\frac{P_{\mathrm{A,B}}(z,t)}{1+\varepsilon P_{\mathrm{A,B}}(z,t)}, \tag{3}$$

$$\pm\frac{\partial P_{\mathrm{CW,CCW}}(z,t)}{\partial z}=\left[\frac{G_{\mathrm{CW,CCW}}(z,t)}{1+\varepsilon P_{\mathrm{A,B}}(z,t)}-\alpha_{\mathrm{int}}\right]P_{\mathrm{CW,CCW}}(z,t), \tag{4}$$

$$\frac{\partial G_{\mathrm{CW,CCW}}(z,t)}{\partial t}=\frac{G_{\mathrm{ss}}-G_{\mathrm{CW,CCW}}(z,t)}{T_{\mathrm{car}}}-\frac{G_{\mathrm{A,B}}(z,t)}{E_{\mathrm{sat}}}\frac{P_{\mathrm{A,B}}(z,t)}{1+\varepsilon P_{\mathrm{A,B}}(z,t)}, \tag{5}$$

where the symbols '+' and '−' refer to the clockwise and counter-clockwise control and clock pulses that are denoted with the subscripts A, B and CW and CCW, respectively. In these equations z is the spatial coordinate along the amplifier and t is the local time measured in a coordinate system moving with the propagating pulse, obtained using the transformation $t\rightarrow t\pm z/u_{\mathrm{g}}$ [43], where u_{g} is the group velocity inside the amplifier related to the speed of light in vacuum, c, through the group refractive index, n_{g}, by $u_{\mathrm{g}}=\frac{c}{n_{\mathrm{g}}}$. The other involved parameters include the SOA small signal gain per unit length, $G_{\mathrm{ss}}=\Gamma\alpha_N N_{\mathrm{tr}}\ (I/I_{\mathrm{tr}}-1)$, where Γ is the confinement factor, α_N the differential gain, N_{tr} the carrier density at transparency, I the injection current, $I_{\mathrm{tr}}=\mathrm{qVN_{tr}}/T_{\mathrm{car}}$ the injected current required for transparency, where q is the electron charge, $V=wdL$ the volume of the SOA active region, with w, d and L being its width, depth and length, respectively, and T_{car} is the carrier lifetime. Also α_{int} is the SOA internal loss per unit length, $E_{\mathrm{sat}}=\hbar\omega\sigma/\alpha_N$ is its saturation energy, where σ is the mode cross-section ($=wd/\Gamma$), $\hbar=h/2\pi$ the normalized Planck's constant and ω the optical carrier frequency and $\varepsilon=\varepsilon_{\mathrm{SHB}}+\varepsilon_{\mathrm{CH}}$ is the nonlinear gain compression factor due to the combined action of the SHB and CH intraband effects.

The four Eqs. (2)–(5) form a system with four unknowns, namely the power and gain of controls A and B and of the CW and CCW clock signal parts, which cannot be solved in closed-form but only numerically. For this purpose and in order to account for the spatial and temporal dependence indicated by the variables (z,t), the SOA length, L, is divided into many sections of constant and finite length $\Delta z=\frac{L}{m}$, whereas the pulses are sampled over their period T_{per} every $\Delta t=\frac{T_{\mathrm{per}}}{k}$ time units so that their profile can be reconstructed at the output. The selection of m and k must be carefully done so that they are integer numbers and at the same time they ensure a high temporal resolution and computational efficiency, although a trade-off can be always done between the last two requirements depending on the available memory and the speed of processing of the computer machine. In particular, the number of longitudinal sections must be larger than 10, otherwise the amount of the differential gain and phase shift induced by the control signals will be overestimated and underestimated, respectively, impeding the correct modeling of XOR [45]. This in turn affects the choice of k, given that the space and time infinitesimal elements are related to each other by $\Delta\mathrm{z}=\mathrm{u_g}\Delta\mathrm{t}$, which implies also that the signals propagate through one amplifier segment during the time interval Δt. For a SOA length of 1000 μm and a typical group refractive index of 3.6, the values $m=120$ and $k=1000$ can provide accurate solutions of Eqs. (2)–(5) with the use of the simple Euler numerical method, which, for each discrete space, 'i', and time section, 'j', can be expressed by

$$P_{i+1,j} = P_{i,j} \pm \Delta z \left.\frac{\mathrm{d}P^{\pm}}{\mathrm{d}z}\right|_{i,j} \quad \text{for } i = 0,1,2,\ldots,m-1 \text{ and } j = 0,1,2,\ldots,k-1, \tag{6}$$

$$G_{i,j+1} = G_{i,j} + \Delta t \left.\frac{\mathrm{d}G}{\mathrm{d}t}\right|_{i,j} \quad \text{for } i = 0,1,2,\ldots,m-1 \text{ and } j = 0,1,2,\ldots,k-1. \tag{7}$$

In other words, for an incoming signal traveling in the positive longitudinal direction (+z), the knowledge of the values of $P(z,t)$ and $G(z,t)$ as well as of their derivative (denoted by $|_{i,j}$) at a given step (i,j) of the algorithm, together with the fact that Eqs. (2)–(5) are essentially coupled in terms of the power and gain, allows to calculate the next values $P(z+\Delta z,t)$ and $G(z,t+\Delta t)$ required at steps $(i+1,j)$ and $(i,j+1)$, respectively. Similarly, for an incoming signal traveling in the negative longitudinal direction $(-z)$, the knowledge of the values of $P(z+\Delta z,t)$ and $G(z,t)$ and of their derivative at a current step $(i+1,j)$ is used to calculate the next values $P(z,t)$ and $G(z,t+\Delta t)$ required at steps (i,j) and $(i+1,j+1)$, respectively. This process is depicted in Fig. 3 and is repeated in an iterative manner until all values are calculated in the spatial–temporal grid $i\,(\Delta z) \times j\,(\Delta t)$. It is thus obvious that in order for this process to start, the necessary initial conditions must be defined and appropriately applied. It is easy to set the initial conditions for the optical power of controls A and B, since these signals take the form of an unchirped, Gaussian-shaped pulse stream

$$P_{\mathrm{A,B}}(t) = \sum_{n=0}^{+\infty} \{C_n\}_{\mathrm{A,B}} \frac{2\sqrt{\ln 2}E_{\mathrm{A,B}}}{\sqrt{\pi}T_{\mathrm{FWHM}}} \times \exp\left[-\frac{(t - nT_{\mathrm{per}} - n_t)^2 4\ln 2}{T_{\mathrm{FWHM}}^2}\right] \tag{8}$$

at the SOA two input facets, $z=0$ and $z=L$, respectively, where n is the number of bits of each data sequence, the single pulse energy is assumed for convenience to be the same for both A and B, i.e., $E_{\mathrm{A,B}} = E_{\mathrm{control}}$, the code $\{C_n\}$ is either 1 or 0 with equal probability 1/2, T_{FWHM} is the pulse width at half-maximum and n_t is a time constant that has been deliberately introduced so that the energy of the first pulse of each sequence is contained entirely in the interval $[0, nT_{\mathrm{per}}]$. Similarly, for the input clock with energy E_{clock} the power is

$$P_{\mathrm{clock}}(t) = \sum_{n=0}^{+\infty} \frac{2\sqrt{\ln 2}E_{\mathrm{clock}}}{\sqrt{\pi}T_{\mathrm{FWHM}}} \times \exp\left[-\frac{(t - nT_{\mathrm{per}} - n_t)^2 4\ln 2}{T_{\mathrm{FWHM}}^2}\right], \tag{9}$$

since it contains only consecutive '1' bits (i.e., $\{C_n\} = 1$). The derivation of the initial gain conditions is not a trivial task, however, due to the fact

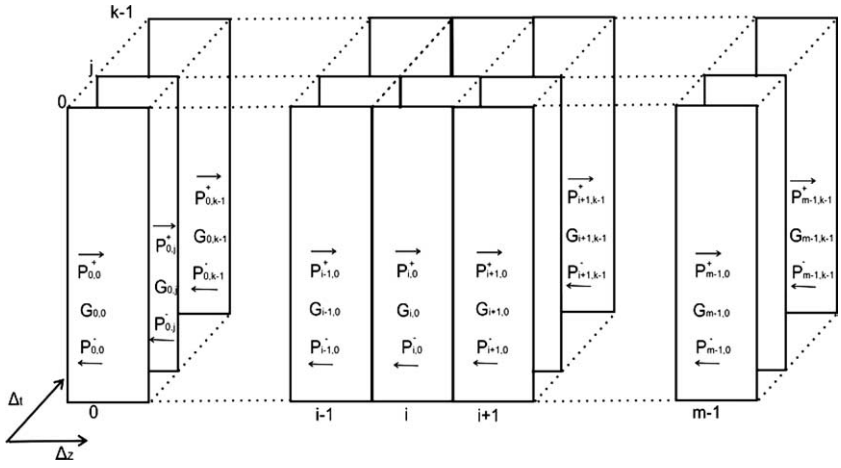

Fig. 3. Schematic diagram of the simulation model. The SOA is divided in discrete longitudinal ('*i*') sections and in each one of them the value of the signal power (P) and gain (G) is calculated for each sample of the pulse ('*j*') based on the knowledge of the preceding value. This stepwise process is separately done for the forward ('+') and the backward ('−') signal propagation.

that the two control signals must be accommodated by a single SOA and not by two distinct ones, as in the case of the MZI-based XOR studies [24–28]. Initially, in each distance segment of the SOA, the first temporal segment in the leading edge of the first bit of control A experiences an unsaturated, small signal gain. After this signal has transit the SOA, the gain begins to recover so that in each distance segment the first temporal segment in the leading edge of the forthcoming bit of control B that arrives after a delay equal to the asymmetry of the loop, T_{asym}, sees a partially recovered gain. This can be determined if the differential equation that describes the gain variation for the control, i.e., (3), is solved by setting the power in the second term of its right-hand side equal to zero so as to simulate the absence of a control signal during the asymmetry delay. In this manner, an ordinary, first order differential equation is obtained, which can be solved analytically to provide the requested initial gain for control B

$$G_{\text{initial }(B)} = G_{\text{ss}} + (G_{\text{A}} - G_{\text{ss}}) \exp\left(-\frac{t_{\text{d,B}} - t_{\text{s,A}}}{T_{\text{car}}}\right), \tag{10}$$

where G_{A} is the gain experienced by the last temporal segment in the trailing edge of control A in the same distance segment at a local time $t_{\text{s,A}} = \frac{z_i}{u_{\text{g}}} = \frac{i\Delta z}{u_{\text{g}}}$ and $t_{\text{d,B}} = T_{\text{asym}} + \frac{L - z_i}{u_{\text{g}}}$ is the local time when the first temporal segment in the leading edge of control B arrives. Note that the term $\frac{L - z_i}{u_{\text{g}}}$ has been introduced to account for the counter-propagation of control B and is a direct consequence of the valid assumption that there is no group velocity mismatch between the signals traveling the SOA. Following this rational, in each distance segment the first temporal segment in the leading edge of the next bit of control A that reaches the SOA after a time period, T_{per}, sees an initial, recovered gain given by

$$G_{\text{initial }(A)} = G_{\text{ss}} + (G_{\text{B}} - G_{\text{ss}}) \exp\left(-\frac{t_{\text{d,A}} - t_{\text{s,B}}}{T_{\text{car}}}\right), \tag{11}$$

where G_{B} is the gain seen by the last temporal segment in the trailing edge of control B in the same distance segment at a local time $t_{\text{s,B}} = \frac{L - z_i}{u_{\text{g}}}$ and $t_{\text{d,A}} = T_{\text{per}} + \frac{z_i}{u_{\text{g}}}$ is the local time when the first temporal segment in the leading edge of control A arrives. This process is similarly repeated for the first temporal segment of each bit in the remaining pairs of control A and B, which experiences a partially recovered gain perturbed by its preceding bit that is calculated using (11) and (10), respectively. Similarly, we can obtain the initial condition for the gain of the first temporal segment of the CW and CCW clock components, which varies depending on the content of the current control bit. According thus to Fig. 2, this may be either a gain that has been saturated by the last temporal segment of the co-propagating control pulse, G_A or G_B, or a recovered gain given by (10) and (11), respectively. In this manner, the time-dependent gains defined as

$$G_{\text{CW}}(t) = \frac{P_{\text{CW}}(z = L, t)}{P_{\text{CW}}(z = 0, t)} \tag{12}$$

and

$$G_{\text{CCW}}(t) = \frac{P_{\text{CCW}}(z = 0, t)}{P_{\text{CCW}}(z = L, t)} \tag{13}$$

can be calculated and replaced in the transfer function of the interferometer [36]

$$T(t) = \frac{1}{4}\Big\{ G_{\text{CW}}(t) + G_{\text{CCW}}(t - T_{\text{asym}}). \\ -2\sqrt{G_{\text{CW}}(t) G_{\text{CCW}}(t - T_{\text{asym}})} \\ \times \cos[\phi_{\text{CW}}(t) - \phi_{\text{CCW}}(t - T_{\text{asym}})] \Big\}, \tag{14}$$

where the time-dependent phase difference between the CW and CCW pulses is

$$\phi_{\text{CW}}(t) - \phi_{\text{CCW}}(t - T_{\text{asym}}) \\ = -\frac{1}{2} a_N \ln\left(\frac{G_{\text{CW}}(t)}{G_{\text{CCW}}(t - T_{\text{asym}})}\right) \tag{15}$$

with a_N being the linewidth enhancement factor. This finally enables to obtain the profile of the XOR output clock pulses from

$$P_{\text{out}}(t) = P_{\text{clock}}(t) T(t). \tag{16}$$

4. Results and discussion

The SOA parameters that are treated as constants throughout the simulation are listed in

Table 2
Description and values of SOA parameters that are fixed in the simulation

Parameter	Symbol	Value
Length of active region	L	1000 μm
Depth of active region	d	250 nm
Width of active region	w	2 μm
Confinement factor	Γ	0.48
Group refractive index	n_g	3.6
Differential gain at $\lambda_{max} = 1550$ nm	α_N	3.7×10^{-20} m^2
Carrier density at transparency	N_{tr}	1.0×10^{24} m^{-3}
Nonlinear gain compression factor	$\varepsilon = \varepsilon_{SHB} + \varepsilon_{CH}$	0.2 W^{-1}
Saturation energy	E_{sat}	1 pJ
Linear internal losses	α_{int}	2000 m^{-1}

Table 2. The cited values are representative of bulk InGaAsP semiconductor materials operating at 1550 nm and are in accordance with theoretical and experimental data provided in the literature [37,42].

In order to assess the performance of the gate at 10 Gb/s, metrics characterizing the quality of switching at the output of the XOR gate were defined and calculated. These are the contrast ratio (CR)

$$\mathrm{CR} = 10\log\frac{P^1_{\mathrm{mean}}}{P^0_{\mathrm{mean}}}, \tag{17}$$

where P^1_{mean} and P^0_{mean} is the mean value of the peak power of '1' and '0', respectively, the amplitude modulation (AM)

$$\mathrm{AM} = 10\log\frac{P^1_{\mathrm{max}}}{P^1_{\mathrm{min}}}, \tag{18}$$

where P^1_{max} and P^1_{min} is the maximum and minimum value of the peak power of '1', respectively, and the extinction ratio (ER)

$$\mathrm{ER} = 10\log\frac{P^1_{\mathrm{min}}}{P^0_{\mathrm{max}}}, \tag{19}$$

where P^1_{min} and P^0_{max} is the minimum and maximum value of the peak power of '1' and '0', respectively. For optimum gate performance, first the contrast ratio must be as high as possible so that the largest fraction of the incoming clock signal exits at the output of the XOR gate, second the amplitude modulation must be as low as possible so that the output '1' have the same level and the pattern effect is negligible, and third the extinction ratio must be as high as possible so that the '1' can be clearly distinguished from the '0'. The priority given to each one of these metrics is not arbitrary but in accordance to its importance. In particular, the contrast ratio is the ultimate performance criterion and imposes the stringent requirements because by definition it characterizes fully the gate across the entire data pattern through the calculation of the mean value of all '1' and '0', whilst the other two metrics can be considered as secondary ones since they account only for the maximum and minimum bit values. Here it must be also noted that the use of these metrics essentially implies that the maximum differential phase shift between the CW and CCW clock pulses does not necessarily have to be equal to the ideal value of π in order to ensure a satisfactory performance. Indeed, if the interferometer is biased for a null with neither of the counter-propagating control pulses present, then it will switch well even if the corresponding phases in its two arms are less than π, provided of course that they are equal [24–26]. This is an important detail from a practical point view because it means that good switching can be achieved with less control energy than ideally needed, which in turn may be useful in reducing gain saturation patterning so as to avoid performance degradation.

According to the principle of operation of the XOR gate and the corresponding model described in Sections 2 and 3, respectively, the parameters of interest include the SOA small signal gain, linewidth enhancement factor and carrier lifetime, the control pulses energy and width and the loop asymmetry. Among these parameters, the energy of the control pulses is of particular importance because it determines the degree of the SOA gain saturation required for optimum operation. At the same time it must be kept as low as possible so that it can be practically provided from commercially available erbium doped fiber amplifiers (EDFAs) and it does not exceed the SOA damage threshold. For this reason, the results for the defined metrics have been obtained by scanning

through the switching (control) energy and each one of the other parameters while keeping the rest of them constant either to a fixed, predefined value or to an optimum one chosen from the observation of the derived simulation curves, namely (a) for the small signal gain, 20 dB (b) for the linewidth enhancement factor, 5, (c) for the carrier lifetime, 100 ps, (d) for the control pulse width, 12 ps, and (e) for the loop asymmetry, 30 ps. This process, which is repeated until all parameters are covered, allows to simultaneously determine the range of the permissible switching energy values as well as the optimum ones and to evaluate the influence of the other parameters on the performance of the XOR gate.

The developed model can handle arbitrary data patterns A and B but these are intentionally selected to be 10111101 and 01101111, respectively, since the same were used in the laboratory implementation at 10 Gb/s [30] and also because both contain consecutive '1' bits so that the pattern dependence of the XOR gate can be more easily demonstrated and evaluated. Here it must be noted that at this stage of the analysis our main goal is to examine and interpret qualitatively the behavior of the gate with respect to the critical parameters rather than focusing on the absolute values of the performance metrics, since this will be done at the end of our study with the completion of the optimization process.

Fig. 4 illustrates the effect on the performance metrics for different small signal gain values. Note that in this curve as well as in the following ones, the lower value of the scanned switching energy is 50 fJ. This value can be obtained by recalling that the control energy must be at least ten times higher than that of the clock, which in turn is set to 5 fJ, in accordance to the experiment [30]. The observation of this figure reveals that the contrast ratio and the extinction ratio degrades when the small signal gain is increased, whilst the opposite occurs for the amplitude modulation. The reason for this is that higher small signal gain values affect drastically the SOA dynamics and can induce a larger differential gain between the counter-propagating clock components, which is accompanied by the creation of a differential phase shift that surpasses π radians. In this manner, more than one local power maxima occur during one bit period, which result in the severe distortion of the switched-out pulses and have thus a negative impact on the performance metrics. This has been experimentally observed, within the frame of characterizing the phase dynamics of bulk SOAs as stand-alone devices [37], as well as theoretically described for the case of all-optical logic [25]. Furthermore, it explains the fact that in the horizontal axis there is an upper limit where the metric curves stop, which varies inversely with the small signal gain and essentially determines the permissible range of values of the control energy. At the same time, the amplitude modulation is decreased, since the more is the small signal gain increased, the stronger is the SOA saturated and the less is its gain dependent on the pulse energy and the data content of the control stream. As a consequence, the clock pulses suffer almost the same gain and their amplification is uniform. This reduction is however very low to justify an increase of the small signal gain and a compromise in the value of the other two metrics so that finally a value of the small signal gain less than 23 dB and preferably around 20 dB is appropriate. In this way we ensure also that the dynamic range of the control energy is wide enough, which is an important issue from a practical point of view, since in a real transmission environment the control signal may be attenuated or exhibit fluctuations due to various propagation impairments so that it must be amplified before entering the XOR gate in a local network node. A final remark that can be made from the observation of Fig. 4, but which holds also for the remaining curves, is that the decrease of the energy while keeping the small signal gain (or one of the rest of the critical parameters, respectively) constant to its preferable value induces the increase of the contrast and extinction ratios, which is more significant for energy values below 100 fJ. At the same time the change of the amplitude modulation is relatively inapparent because, due to the presence of the two control beams, the SOA is brought to a saturation degree that enables to partially compensate the dependence of the gate on the statistics of '1' and '0'. This additionally justifies the fact that the value of 50 fJ per control pulse that must be ideally provided

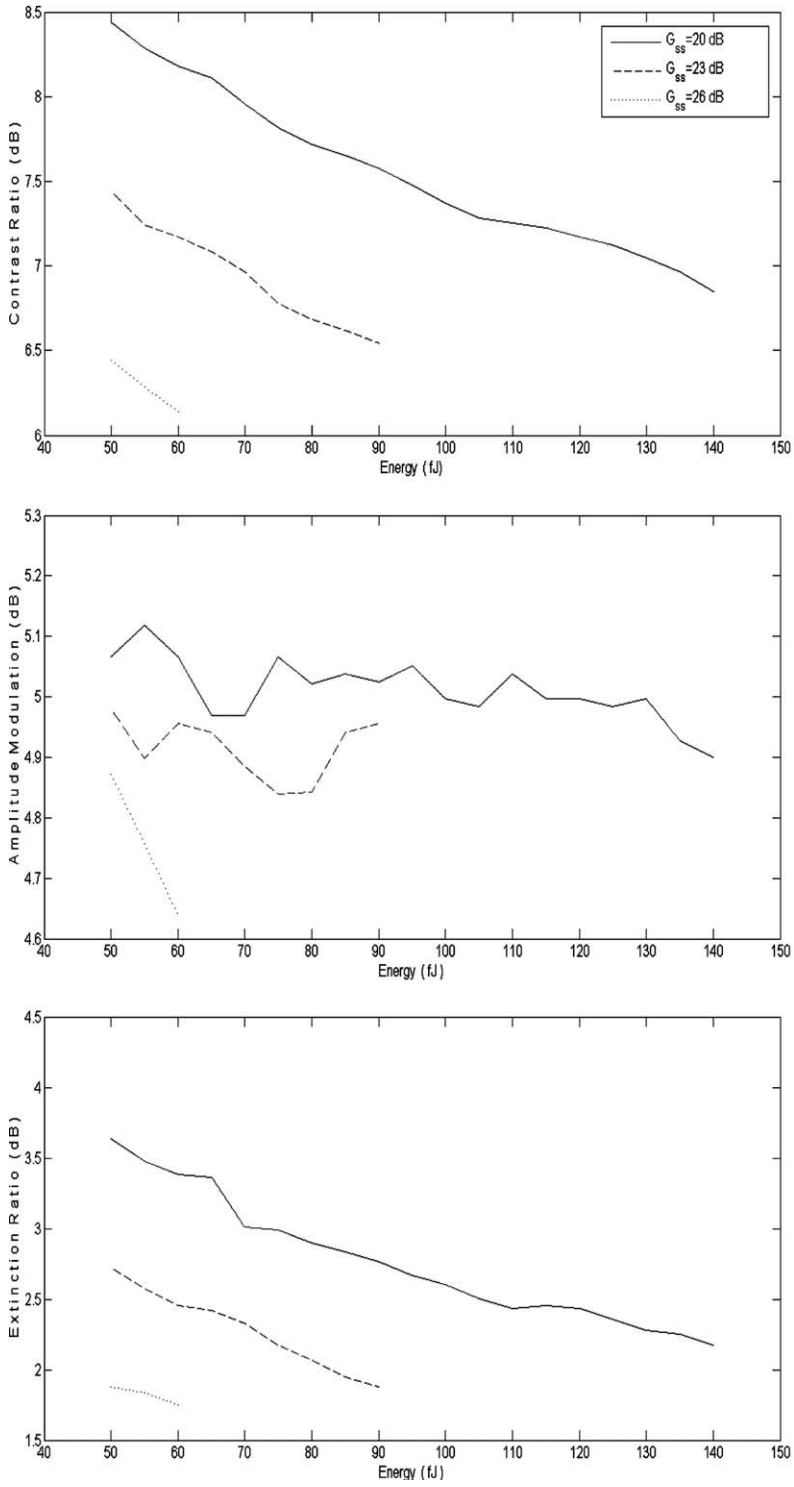

Fig. 4. Metrics variation versus SOA small signal gain.

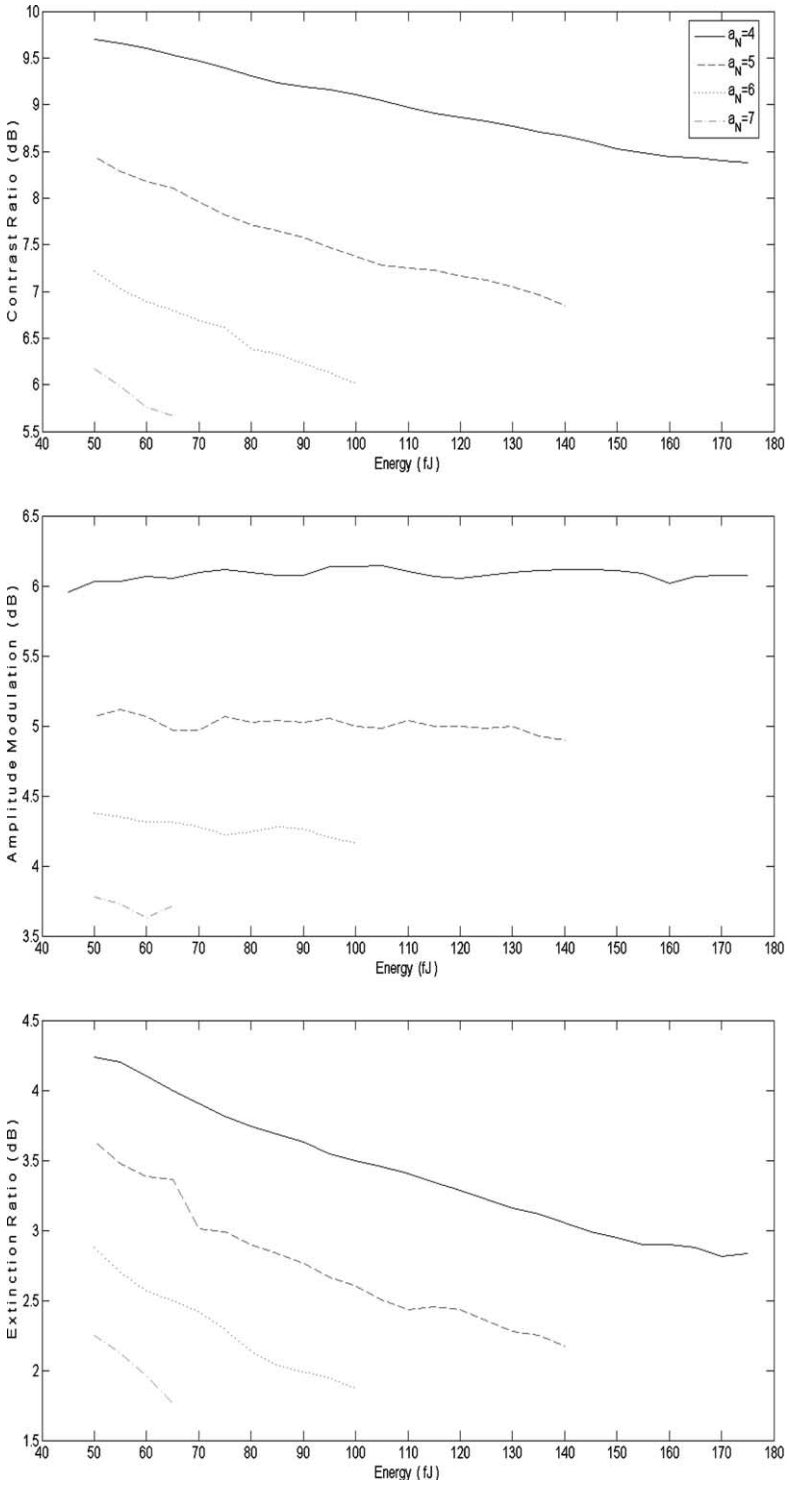

Fig. 5. Metrics variation versus SOA linewidth enhancement factor.

according to Fig. 4 in order to obtain the highest contrast and extinction ratio is almost twice the predicted energy required for the operation of the AND gate [46].

Fig. 5 depicts the influence of the linewidth enhancement factor on the performance metrics and as it can be seen, a small value of this parameter is necessary in order to obtain a high contrast and extinction ratio. This can be understood by referring to Eq. (15), in which the linewidth enhancement factor plays a major role in determining the extent of the phase difference between the counter-propagating clock pulses and hence the quality of switching. For large values thus of this parameter, as for example $a_N = 7$, not only the phase shift will exceed by far π radians, but as it can be also seen in Fig. 6, the gate's switching window that is opened during the period of the maximum XOR output bit '1' will be distorted and severely broadened resulting in serious intersymbol interference and performance degradation. In this manner, a situation similar to that described for the case of the small signal gain occurs, which becomes even worse when the control energy overcomes its upper limit that varies inversely with the linewidth enhancement factor. On the other hand, the amplitude modulation is improved with the increase of the linewidth enhancement factor because this results in a larger phase change and increases accordingly the level of the output bits '1', so that their magnitude is equalized. Nevertheless, a value of a_N no higher than 6 must be selected due to the priority given to the contrast ratio, and the investigation of the remaining of the parameters will enable to identify which of them has the most significant influence on the amplitude modulation. It must be also noted that Fig. 5 enables to assess and confirm the validity of our model by comparing the information contained in the contrast ratio curve with the available experimental results [30]. More specifically, for a control energy of 100 fJ that was used in the experiment and $a_N = 4$, the simulated value of the contrast ratio is approximately 9.2 dB, which in turn is close to the experimental one of 10.4 dB. The existing discrepancy is due to the fact that the theoretical contrast ratio has been calculated using the more complete and accurate definition of (17), in contrast to the experimental value that has been derived by taking into account only the single, best quality pair of the output '1' and '0' bits.

The SOA carrier lifetime is a key operational factor that affects decisively the performance of the XOR gate. Fig. 7 demonstrates indeed that an increase of its value by even half from 50 to 100 ps causes a drastic change on the defined metrics. Unlike thus the previous cases where the contrast and extinction ratio varied in opposite

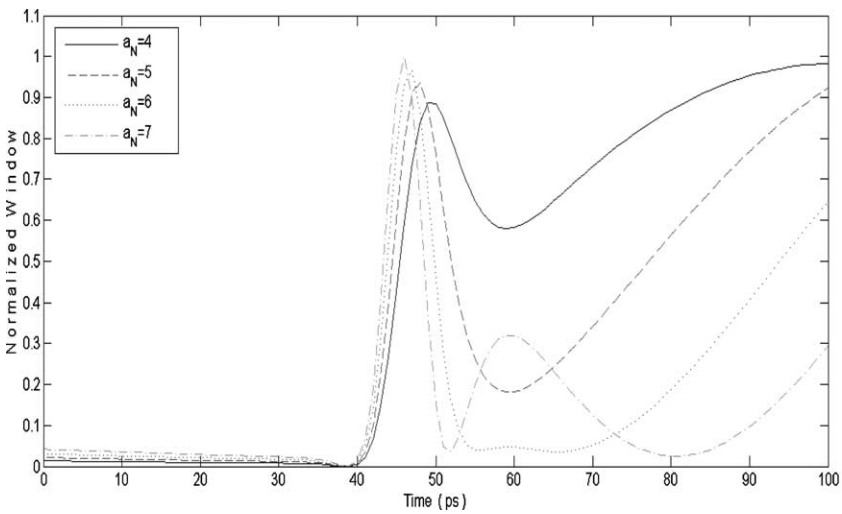

Fig. 6. Normalized switching window versus SOA linewidth enhancement factor.

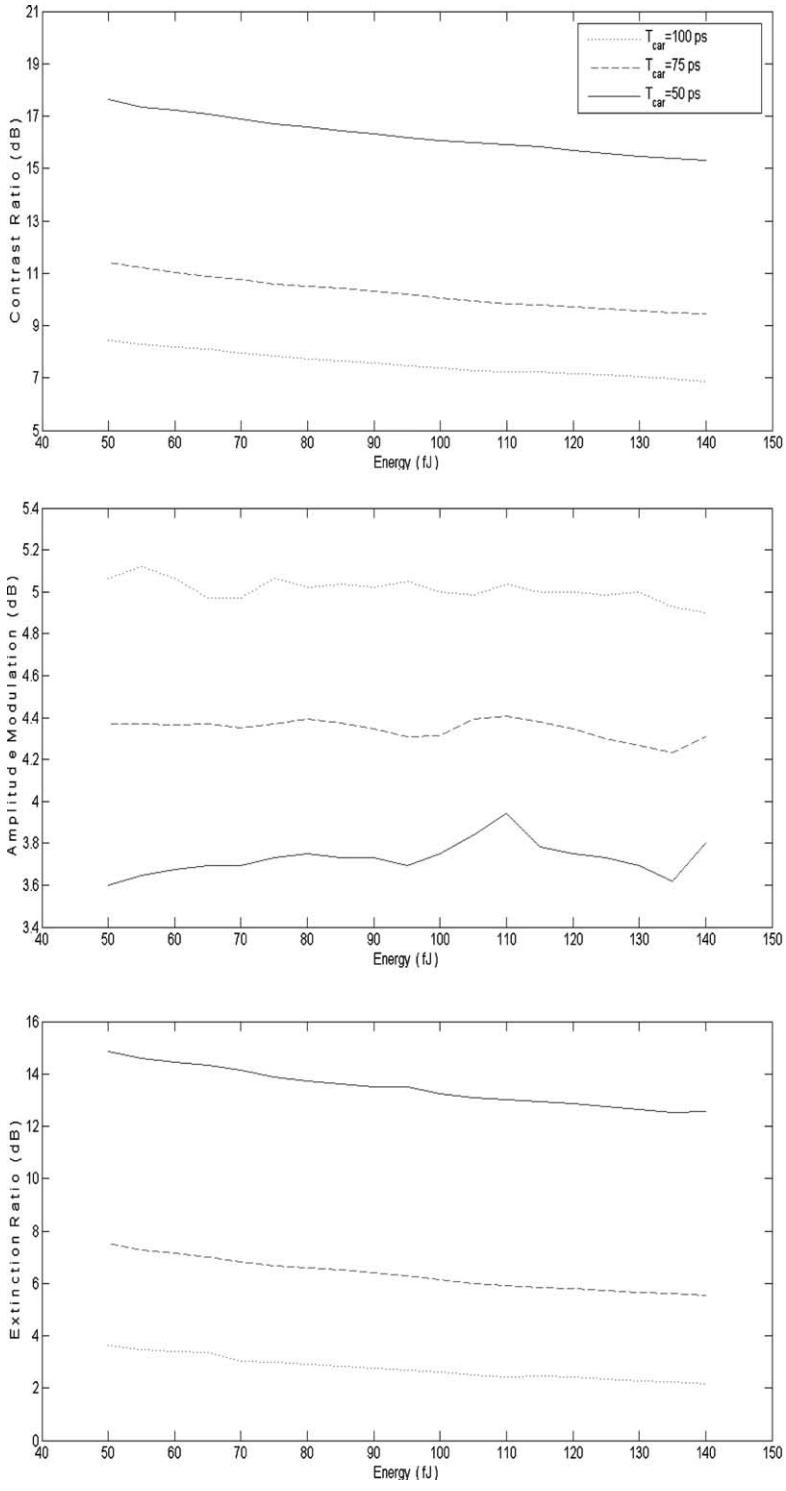

Fig. 7. Metrics variation versus SOA carrier lifetime.

manner compared to the amplitude modulation for a change of the small signal gain and the linewidth enhancement factor, now all metrics are significantly deteriorated. However, particular attention must be given to the increase of the amplitude modulation because it results in a serious pattern effect at the output of the gate. This phenomenon is ascribed to the advent of the '1' and '0' bits contained in the data-modulated control pulse trains, which during their period cause a rapid drop of the SOA gain or allow it to recover, respectively. This effect is more intense at the time intervals where there is a change from '1' to '0' and vice versa, since a '1' saturates strongly the SOA and the '0' that follows leaves enough time for gain recovery so that the next '1' exhibits a different gain and phase change than the previous '1'. Moreover, continuous '0' bits help the gain to rise further whilst continuous '1' bits impede the gain to recover fully. The result is that the gain and thus the amplitude of a specific bit depends on the preceding bits, causing significant amplitude distortion [47]. In this manner, the value of the XOR output bit cannot be correctly distinguished at the receiver end leading to an increased bit error rate (BER) and in performance degradation. In order to combat this effect and its deleterious consequences, the carrier lifetime must be reduced so that it is smaller than the specific bit period and the gain can recover completely between consecutive pulses. The most direct method for achieving this goal is by increasing the SOA injection current and length [48] but at a double cost. First, high bias currents can be provided only by using more costly, complex and power-consuming current sources with the associated driving electronics. Second, longer SOA lengths result in higher ASE [37], which in turn alters undesirably the saturation behavior of the gate so that the output signal-to-noise-ratio is degraded, and impose a significant limit on the maximum data rate of operation [49]. For this reason, several efficient gain recovery enhancement techniques have been deployed during recent years, such as the injection of a continuous wave strong holding beam [50] or of an assist light near the SOA transparency point [51]. The implementation of these techniques is not a trivial task, however, since they are accompanied by an unavoidable reduction of the small signal gain, which in turn affects negatively the creation of the necessary differential phase shift. For this reason, a compromise is required between speed and the available phase change, which can be achieved by carefully adjusting the power and properly selecting the wavelength of the continuous-wave pumping beam that is responsible for the reduction of the recovery time [52], but at the inevitable cost of increased complexity. An alternative solution is to use the novel technology of quantum-dot SOAs [53], which due to the combination of several attractive features, such as the very wide gain bandwidth, the inhomogeneous broadened gain spectra, the high saturation power and the fast recovery time of the order of hundreds of fs, has attracted intense research efforts that are starting to bear fruits in the field of all-optical switching [54,55]. Finally, it should be noted that all these approaches can address more efficiently the problem of pattern effect if they are combined with the appropriate control pulse coding. In fact, results have shown that due to its constant intensity nature, the return-to-zero differential phase-shifted keying (RZ-DPSK) modulation format can effectively alleviate the pattern-dependent distortion in SOA-based configurations with negligible power penalty, and thus it is more robust than the conventional RZ ON–OFF keying scheme for use in OTDM systems [56].

The variation of the metrics against the width of the control pulses is plotted in Fig. 8. Initially, we notice that no safe results can be extracted concerning the influence of this parameter when the energy is kept constant, since the different curves in each metric are very close to each other and cannot be clearly distinguished. This is an imperfection of the adopted simulation method attributed to the fact that the model treats time in a discrete manner and not continuously in order to produce numerical instead of analytical solutions. A reduction thus of the FWHM that is inserted in (8) and (9) means that fewer pulse samples contribute to the switching procedure, which in turn affects the accuracy of the corresponding results. Nevertheless, Fig. 8 can still provide useful information when the energy is varied and as it can be seen in that case, a specific contrast or extinction

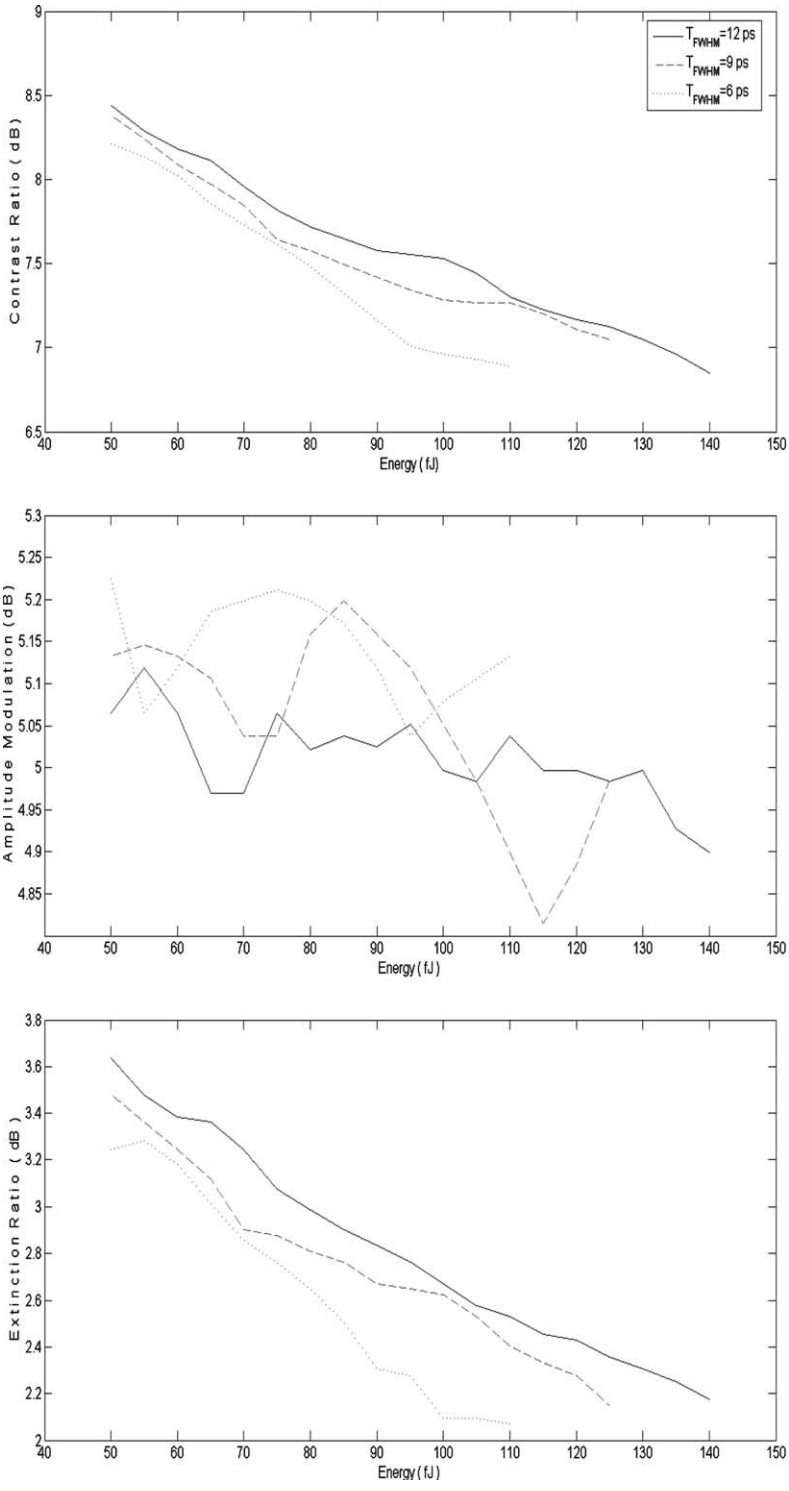

Fig. 8. Metrics variation versus control pulse width (FWHM).

ratio value can be achieved with less energy for a shorter pulse width, whilst the amplitude modulation is rather insensitive for the reasons already explained. This happens because a shorter pulse passes quicker through the SOA enhancing thus the rapid depletion of carriers and resulting in a steeper transition from the lower to the higher saturated gain values. For this reason, the necessary gain change and hence the accompanying phase shift between the CW and CCW pulses can be achieved using a smaller energy. In contrast, a longer pulse needs more time to traverse the SOA and cause a change in its optical properties, so that an energy increase is inevitable to compensate for the small difference between the gains and phases of the CW and CCW pulses. However, care must be taken concerning the extent of the pulse width decrease, since for values less than 2 ps the intraband effects become more pronounced and have a negative effect on the gate's switching window, which may even take the form of an oscillating multi-peak structure [57].

Finally, the simulated metrics as a function of the asymmetry are presented in Fig. 9, which illustrates that a better performance is achieved when it approaches the upper limit of Eq. (1) and takes values near half the bit period. This happens because in that case the CCW clock pulse is appropriately delayed with respect to its CW counterpart so that a sufficient gain and phase difference can be created independently of the logical combinations of A and B. This is an attractive feature from an OTDM network perspective because a higher asymmetry results in a wider switching window with respect to the pulse width so that the performance of the gate can be improved [58] while simultaneously ensuring a high tolerance to a possible jitter of the incoming control signals [34]. In contrast, the decreased values of this parameter must be avoided, since then the difference between the gains and hence the output of the gate is small with negative consequence on the performance metrics.

From the above simulation results, it can be summarized that in order to optimize the defined performance metrics for XOR operation at 10 Gb/s, the small signal gain must be less than 23 dB, the linewidth enhancement factor at maximum 6, the carrier lifetime less than 100 ps but higher than the asymmetry, the width of the control pulses as short as possible but higher than 2 ps and the loop asymmetry near 50 ps, while the switching energy must lie in the range 50–100 fJ. This essentially means that the combination of the optimum values of these key parameters is not unique. By choosing for example $G_{ss} = 20$ dB, $a_N = 6$, $T_{car} = 50$ ps, T_{FWHM} 6 ps, $T_{car} = 45$ ps and a control energy of 70 fJ so that these operational conditions are satisfied, the contrast ratio, the amplitude modulation and the extinction ratio are 15.5, 1.1 and 14.5 dB, respectively, which are more than adequate for all-optical logic applications. The XOR logic can be thus executed correctly bit by bit while keeping minimum the pattern effect on the switched-out pulses, as shown in the left-hand side of Fig. 10. On the contrary, if the critical parameters deviate from their optimum value, then a strong pattern effect is introduced that severely degrades the quality of switching, as shown in the right-hand side of Fig. 10, where there is a notable amplitude variation between the bits '1' and the '0' bits are not completely extinguished.

The differences in the amplitudes of the output pulses reveal the pattern dependence of the XOR gate. However, unlike the case of a single SOA driven by only one data train or of two SOAs with a separate modulated stream inserted in each one of them, as for example in the MZI XOR gate [24–28], the strain imposed on the gain dynamics of the SOA in the Sagnac gate is greater since it is subject to two intense pulse trains that enter it alternately with a time delay defined by the loop asymmetry. In the XOR result of Fig. 10, the pattern effect is introduced between the 2nd, 4th and 7th output bits. This can be better understood for the case of the two specific data patterns A and B used throughout the model by considering again the XOR operation mechanism described in Fig. 2. If we examine thus the situation that occurs in the 2nd bit period of A and B, we notice that the CW pulse suffers a highly recovered gain due to the absence of a bit in the specific interval of A, $\{A_2\} = \{0\}$, but also because a bit is missing in the previous temporal position of B, $\{B_1\} = \{0\}$. On the other hand, the CCW pulse encounters a gain that is strongly saturated by the second bit

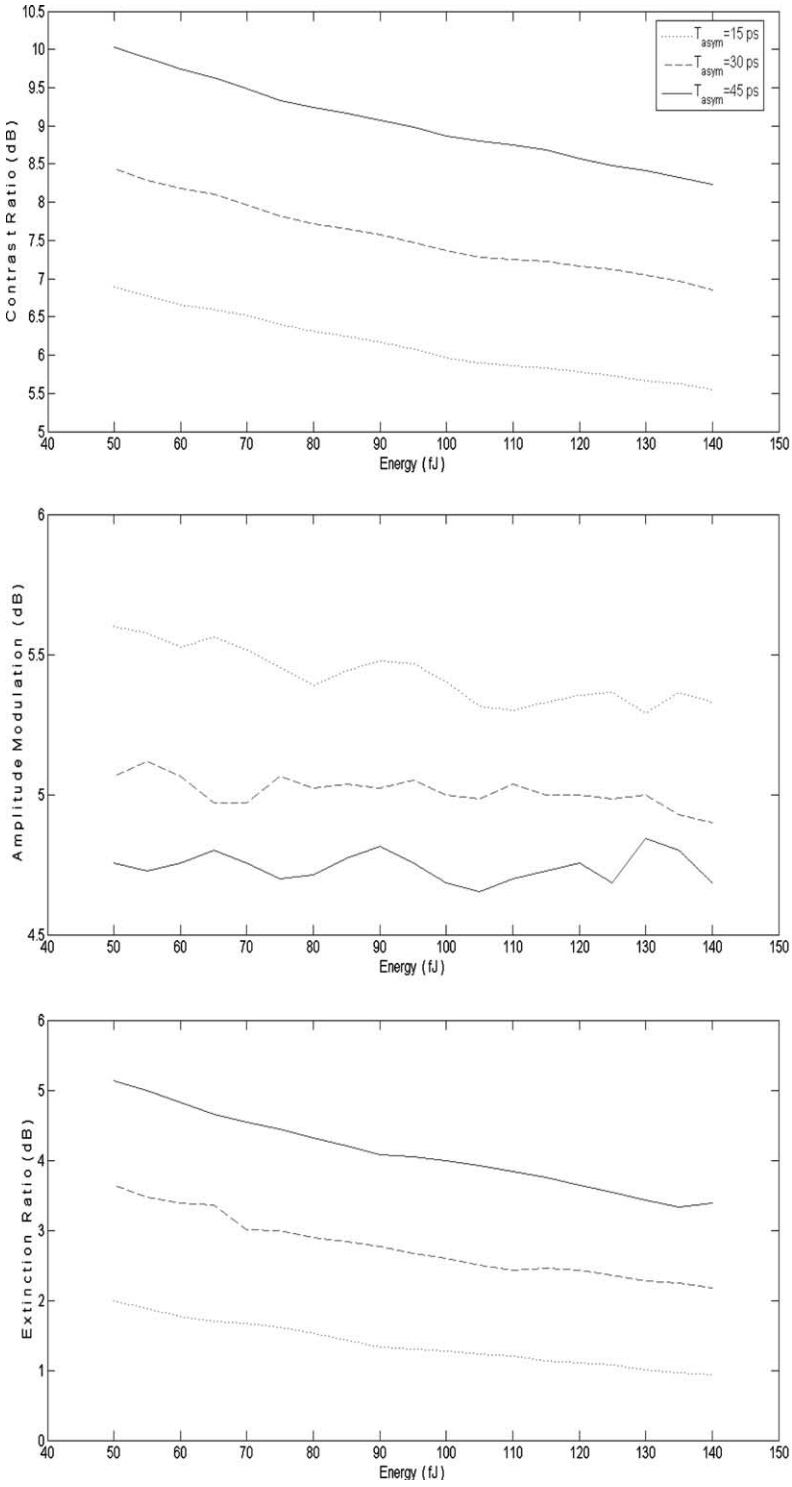

Fig. 9. Metrics variation versus Sagnac loop asymmetry.

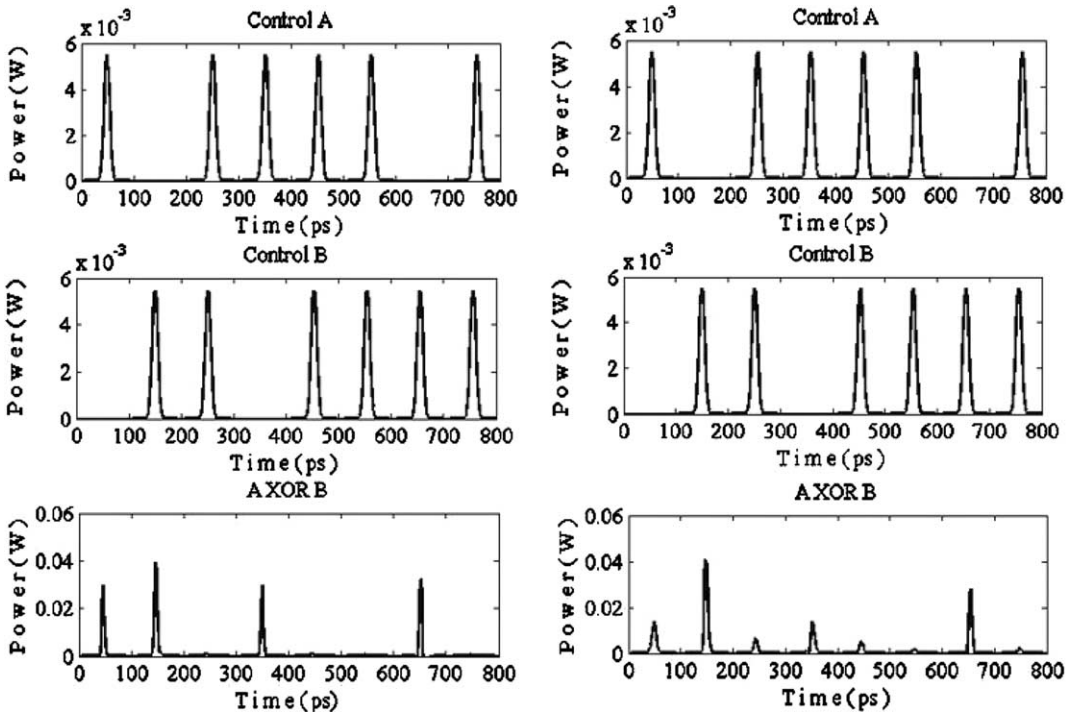

Fig. 10. Simulation results of the XOR operation (bottom) between control data 10111101 (top) and 01101111 (middle) for optimum (left-hand side) and non-optimum (right-hand side) critical parameter values. Note that due to the use of the time constant n_t in (8) and (9), the peak of the pulses has been shifted to the right of the time axis and positioned at the middle of each period interval.

of B, $\{B_2\} = \{1\}$. In this manner, a large gain difference is created between the two clock counterparts, which is translated to a higher amplitude of the resulting bit '1' over the rest bits '1' in the output sequence. In fact, the '1' that is produced in the 4th bit period is less intense because, according to the same rational, the CW pulse exhibits a gain which is heavily saturated by bit $\{B_3\} = \{1\}$ and the subsequent $\{A_4\} = \{1\}$, whilst the CCW pulse a gain that has not had enough time to recover so that the induced gain difference is comparatively lower. However, the output '1' in the 7th bit period slightly surpasses that in the 4th bit period because in that case the succession of bits $\{B_6\} = \{1\}$ and $\{A_7\} = \{0\}$ allows a longer effective time for gain recovery so that although the CCW pulse sees a saturated gain by bit $\{B_7\} = \{1\}$, this has been dropped from a higher level with direct influence on the gain difference and hence on the output amplitude. We realize thus that in the SOA-assisted Sagnac XOR gate the pattern effect is not a matter of the order and the logical value of the bits in each separate control stream. Instead, it depends on the saturation process that takes place in the bit pairs whose content differs, which in turn is affected by the bit that precedes such a pair. This underlies once again the need for deploying gain recovery acceleration techniques or devices so as to suppress the pattern effect and improve the XOR output.

5. Conclusion

In conclusion, we have conducted an extensive theoretical analysis to investigate the operating characteristics of an all-optical XOR gate based on a SOA-assisted Sagnac interferometer. For this purpose, we have developed a comprehensive model consisting of a set of equations that describe pulse propagation and amplification through a SOA in an interferometric switch. The numerical

solution of these equations has allowed to assess the effect of several critical parameters, which include the SOA small signal gain, linewidth enhancement factor and carrier lifetime, the switching pulses energy and width and the Sagnac loop asymmetry, on the performance of the gate. The obtained simulation results are in accordance to the experimental ones, which in turn proves the validity of the model. Furthermore, it has been possible on the basis of these results to extract useful design rules that must be followed and identify the major imposed limitations that must be considered concerning the selection of these parameters, so that the metrics that determine the quality of switching can be optimized. The calculations showed that among the involved parameters, the SOA carrier lifetime is the most crucial and imposes the stricter limitation on the performance of the gate, because depending on its value it can aggravate or mitigate the pattern effect observed on the switched-out pulses. On the other hand, the rest of the parameters can be provided with the state-of-the-art photonics technology without other restriction. For this reason, it is necessary to deploy either complex gain recovery enhancement techniques or alternatively exploit the novel technology of quantum dot SOAs so as to effectively reduce the carrier lifetime. Provided thus that all the parameters are appropriately selected, the SOA-assisted Sagnac XOR gate can yield a fairly high performance at 10 Gb/s. The adopted method of analysis can be applied for studying more complicated all-optical circuits of non-trivial functionality whose operation relies on the XOR gate.

References

[1] R. Ramaswami, IEEE Commun. Mag. 40 (2002) 138.
[2] A.H. Gnauck, G. Raybon, P.G. Bernasconi, J. Leuthold, C.R. Doerr, L.W. Stulz, IEEE Photon. Technol. Lett. 15 (2003) 1618.
[3] T. Houbavlis, K.E. Zoiros, M. Kalyvas, G. Theophilopoulos, C. Bintjas, K. Yiannopoulos, N. Pleros, K. Vlachos, H. Avramopoulos, L. Schares, L. Occhi, G. Guekos, J.R. Taylor, S. Hansmann, W. Miller, J. Lightwave Technol. 23 (2005) 781.
[4] K.L. Hall, K.A. Rauschenbach, Electron. Lett. 32 (1996) 1214.
[5] S.A. Hamilton, B.S. Robinson, IEEE Photon. Technol. Lett. 14 (2002) 209.
[6] R. Clavero, J.M. Martinez, F. Ramos, J. Martí, Opt. Exp. 12 (2004) 4326.
[7] K.E. Zoiros, T. Houbavlis, M. Kalyvas, Opt. Quantum Electron. 36 (2004) 1005.
[8] J.H. Kim, Y.T. Byun, Y.M. Jhon, S. Lee, D.H. Woo, S.H. Kim, Opt. Commun. 218 (2003) 345.
[9] A.J. Poustie, K.J. Blow, A.E. Kelly, R.J. Manning, Opt. Commun. 162 (1999) 37.
[10] T.J. Xia, Y. Liang, K.H. Ahu, J.W. Lou, O. Boyraz, Y.-H. Kao, X.D. Cao, S. Chaikamnerd, J.K. Anderson, M.N. Islam, IEEE Photon. Technol. Lett. 10 (1998) 153.
[11] B.S. Robinson, S.A. Hamilton, S.J. Savage, OFC Proc. ThY2 (2002) 561.
[12] H.J. Lee, C.S. Park, IEICE Trans. Commun. E84B (2001) 330.
[13] J.H. Kim, Y.M. Jhon, Y.T. Byun, S. Lee, D.H. Woo, S.H. Kim, IEEE Photon. Technol. Lett. 14 (2002) 1436.
[14] H. Soto, D. Erasme, G. Guekos, IEEE Photon. Technol. Lett. 13 (2001) 335.
[15] K. Chan, C.-K. Chan, L.K. Chen, F. Tong, IEEE Photon. Technol. Lett. 16 (2004) 897.
[16] S. Kumar, A.E. Willner, LEOS Annual Meeting Proc. ThU2 (2004) 913.
[17] C. Bintjas, M. Kalyvas, G. Theophilopoulos, T. Stathopoulos, H. Avramopoulos, L. Occhi, L. Schares, G. Guekos, S. Hansmann, R. Dall'Ara, IEEE Photon. Technol. Lett. 12 (2000) 834.
[18] T. Fjelde, D. Wolfson, A. Kloch, B. Dagens, A. Coquelin, I. Guillemot, F. Gaborit, F. Poingt, M. Renaud, Electron. Lett. 36 (2000) 1863.
[19] H. Chen, G. Zhu, Q. Wang, J. Jaques, J. Leuthold, A.B. Piccirilli, N.K. Dutta, Electron. Lett. 38 (2002) 1271.
[20] S. Lee, J. Park, K. Lee, D. Eom, S. Lee, J.H. Kim, Jpn. J. Appl. Phys. 2 (41) (2002) L1155.
[21] R.P. Webb, R.J. Manning, G.D. Maxwell, A.J. Poustie, Electron. Lett. 39 (2003) 79.
[22] K.E. Stubkjaer, IEEE J. Select. Top. Quantum Electron. 6 (2000) 1428.
[23] B. Dagens, A. Labrousse, R. Brenot, B. Lavigne, M. Renaud, OFC Proc. ThX1 (2003) 582.
[24] M. Zhang, Y. Zhao, L. Wang, J. Wang, P. Ye, Opt. Commun. 223 (2003) 301.
[25] T. Houbavlis, K.E. Zoiros, G. Kanellos, C. Tsekrekos, Opt. Commun. 232 (2004) 179.
[26] L. Wang, M. Zhang, Y. Zhao, P. Ye, Microwave Opt. Technol. Lett. 40 (2004) 173.
[27] Q. Wang, G. Zhu, H. Chen, J. Jaques, J. Leuthold, A.B. Piccirilli, N.K. Dutta, IEEE J. Quantum Electron. 40 (2004) 703.
[28] S. Randel, A.M. de Melo, K. Petermann, V. Marembert, C. Schubert, J. Lightwave Technol. 22 (2004) 2808.
[29] I. Glesk, R.J. Runser, P.R. Prucnal, Acta Phys. Slovaca 51 (2001) 151.

[30] T. Houbavlis, K. Zoiros, A. Hatziefremidis, H. Avramopoulos, L. Occhi, G. Guekos, S. Hansmann, H. Burkhard, R. Dall'Ara, Electron. Lett. 35 (1999) 1650.
[31] T. Houbavlis, K.E. Zoiros, Opt. Eng. 42 (2003) 3415.
[32] G. Swift, Z. Ghassemlooy, A.K. Ray, J.R. Travis, Microwave Opt. Technol. Lett. 15 (1997) 380.
[33] X.B. Liu, P.D. Ye, Microwave Opt. Technol. Lett. 24 (2000) 374.
[34] H. Shi, J. Lightwave Technol. 20 (2002) 682.
[35] Y. Zhou, J. Wu, J. Lin, LEOS Annual Meeting Proc. ThDD3 (2004) 995.
[36] R.J. Runser, D. Zhou, C. Coldwell, B.C. Wang, P. Toliver, K.-L. Deng, I. Glesk, P.R. Prucnal, Opt. Quantum Electron. 33 (2001) 841.
[37] L. Schares, C. Schubert, C. Schmidt, H.G. Weber, L. Occhi, G. Guekos, IEEE J. Quantum Electron. 39 (2003) 1394.
[38] D. Zhou, K. Kang II, I. Glesk, P.R. Prucnal, J. Lightwave Technol. 17 (1999) 298.
[39] P. Borri, S. Scaffetti, J. Mørk, W. Langbein, J.M. Hvam, A. Mecozzi, F. Martelli, Opt. Commun. 164 (1999) 51.
[40] J.M. Tang, K.A. Shore, IEEE J. Quantum Electron. 34 (1998) 1263.
[41] K. Obermann, S. Kindt, D. Breuer, K. Petermann, J. Lightwave Technol. 16 (1998) 78.
[42] R. Gutiérrez-Castrejón, L. Schares, L. Occhi, G. Guekos, IEEE J. Quantum Electron. 36 (2000) 1476.
[43] G.P. Agrawal, N.A. Olsson, IEEE J. Quantum Electron. 25 (1989) 2297.
[44] J.M. Tang, P.S. Spencer, K.A. Shore, Proc. Optoelectron. 145 (1998) 83.
[45] W.M. Wong, K.J. Blow, Opt. Commun. 215 (2003) 169.
[46] T. Houbavlis, K.E. Zoiros, Opt. Eng. 43 (2004) 1622.
[47] R.J. Manning, A.D. Ellis, A.J. Poustie, K.J. Blow, J. Opt. Soc. Am. B 14 (1997) 3204.
[48] F. Girardin, G. Guekos, A. Houbavlis, IEEE Photon. Technol. Lett. 10 (1998) 784.
[49] K.L. Hall, B.S. Robinson, CLEO Proc. CTuW1 (1999) 214.
[50] R. Inohara, K. Nishimura, M. Tsurusawa, M. Usami, IEEE Photon. Technol. Lett. 15 (2003) 1192.
[51] J.L. Pleumeekers, M. Kauer, K. Dreyer, C. Burrus, A.G. Dentai, S. Shunk, J. Leuthold, C.H. Joyner, IEEE Photon. Technol. Lett. 14 (2002) 12.
[52] H. Wei, H. Dexiu, S. Junqiang, L. Deming, Opt. Commun. 214 (2002) 335.
[53] M. Sugawara, T. Akiyama, N. Hatori, Y. Nakata, H. Ebe, H. Ishikawa, Meas. Sci. Technol. 13 (2002) 1683.
[54] A.V. Uskov, E.P. O'Reilly, R.J. Manning, R.P. Webb, D. Cotter, M. Laemmlin, N.N. Ledentsov, D. Bimberg, IEEE Photon. Technol. Lett. 16 (2004) 1265.
[55] H. Sun, Q. Wang, H. Dong, N.K. Dutta, Opt. Exp. 13 (2005) 1892.
[56] K. Chan, C.-K. Chan, L.K. Chen, F. Tong, IEEE Photon. Technol. Lett. 15 (2003) 1264.
[57] J.M. Tang, P.S. Spencer, K.A. Shore, J. Lightwave Technol. 16 (1998) 86.
[58] T. Houbavlis, K.E. Zoiros, Opt. Quantum Electron. 35 (2003) 1175.